# CHAPTER 10

# GUIDING AND AMPLIFICATION OF LIGHT DUE TO SILICON NANOCRYSTALS EMBEDDED IN WAVEGUIDES

Tomáš Ostatnický, Martin Rejman, and Jan Valenta

*Department of Chemical Physics and Optics, Faculty of Mathematics and Physics, Charles University, Ke Karlovu 3, CZ-121 16 Prague 2, Czech Republic*

Kateřina Herynková, Ivan Pelant

*Institute of Physics, Academy of Sciences of the Czech Republic, v.v.i., Cukrovarnická 10, CZ-162 53 Prague 6, Czech Republic*

In this chapter, we summarize our progress in both experimental and theoretical investigations of spontaneous emission of silicon nanocrystals embedded in planar waveguides. We give an overview of our photoluminescence measurements which reveal peculiar phenomena like spectral filtering of the signal or polarization splitting of the spectra. We discuss possible interpretations of the observed events and we present a model which is capable of explanation of all the peculiarities. Finally we apply the model in order to investigate the consequences of the waveguiding effects for the light amplification, propagation and spectroscopy measurements.

## 1. Introduction

Nanocrystalline silicon attracts attention in many research groups because of its prospective applicability in optoelectronic devices as an amplifier or a source of light. High concentrations of Si nanocrystals and high optical quality of the active media are desired to get a positive net optical gain. To accomplish the requirements, samples prepared by using various methods have been checked in experiments addressing optical

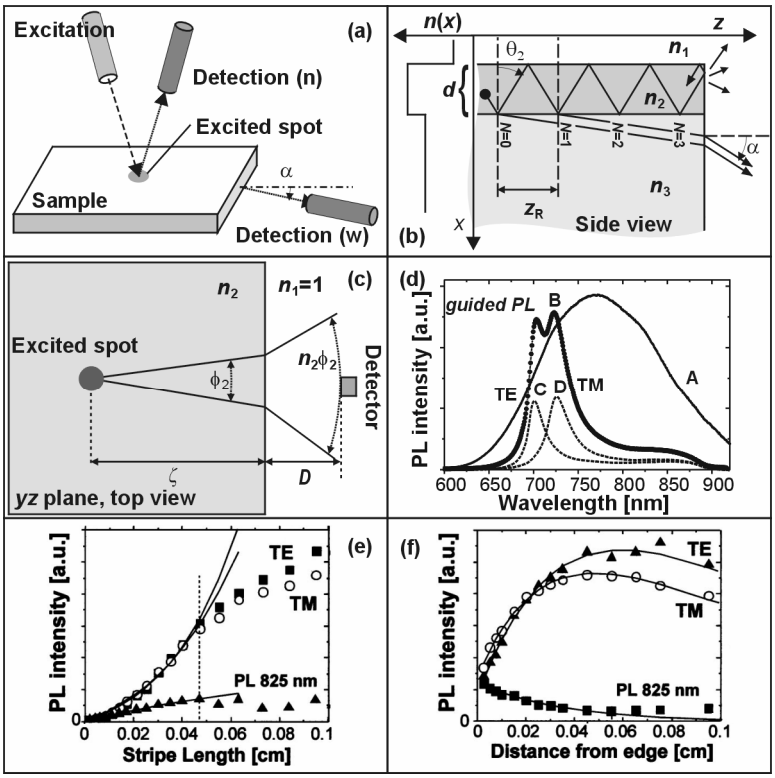


Fig. 1. (a) Experimental setup with two possible detection positions: standard (n) and waveguiding (w). (b) Propagation and decoupling of substrate modes; (c) sketch for derivation of coupling coefficients; (d) measured PL in standard (A) and waveguiding geometry (B) and in the waveguiding geometry with a linear polarizer (C,D); (e) measured ASE intensity at various spectral positions: at maxima of TE and TM modes and at 825 nm; (f) measured SES signal at the same spectral positions.[2]

gain: $Si^+$ ion implantation,[1,2] plasma–enhanced chemical vapour deposition,[3] reactive Si deposition,[4] magnetron sputtering[5] or others.[6] The samples prepared by these methods have a form of a thin $SiO_2$ layer (few micrometers thick) doped with Si nanocrystals, located on an optically thick Si or silica substrate. The thin "sheet" which contains nanocrystals then may reveal waveguiding properties because of the refractive index mismatch between the sheet and the $SiO_2$ matrix.

The waveguiding property and the "planar" method of fabrication are advantageous for integration of components in optoelectronics, however, it was found that the characteristics of a photoluminescence (PL) emission of the samples are strongly affected by the presence of the waveguide[2,7-12] and depend upon many parameters of the sample preparation.[9,13,14] We have investigated the PL emission of the Si nanocrystals embedded in waveguides both theoretically and experimentally and we summarize our findings in this chapter.

Effects connected with waveguiding in the implanted samples were firstly discussed in detail by our group[2] and confirmed by an independent observation of the same phenomenon on samples prepared by reactive deposition[7] — in the experiments, photoluminescence from the active layer was collected in the "waveguiding" configuration along the layer with Si nanocrystals (see Fig. 1a for the experimental setup). Compared to a PL spectrum collected in the standard configuration (perpendicular to the sample plane), the spectra reveal a disturbance of the wide PL band and a narrowing to one or more pairs of modes resolved in linear polarization (Fig. 1d). The unusual behaviour of the PL spectra was observed in measurements of amplified spontaneous emission (ASE) using the variable stripe length (VSL) method[2,15] where the shape of the ASE curves strongly depended on the wavelength of detected radiation (see Figures 1e-1f).

Numerical analysis of the problem shows that the spectrally narrow modes are formed very close to the cut-off frequency of the waveguide. This fact has led us to the interpretation[8,16,17] of our observations, namely, that the modes are formed by the waves leaking from the waveguide core slightly below the critical angle for the total reflection on the core/substrate boundary. Another interpretation was given by Khriachtchev *et al.*[7,9,10] in terms of particular guided modes which are spatially delocalized near the cut-off frequency and therefore their losses due to absorption in the core are lower than losses of the ordinary guided modes.

In this chapter, we develop a consistent model which predicts the observed behaviour and we discuss both hypotheses (delocalization and wave leaking) in order to find which of them plays a major role in formation of the PL spectra. We then show the consequences of the

waveguiding and related effects for spectroscopic measurements, applications in optics and optoelectronics, gain measurements and construction of a lasing device. After a short introduction to waveguide theory in section 2, our model is discussed in more details in section 3. Since the original model does not take into account propagation of the modes along the waveguiding layer, we present its phenomenological extension in section 4, and in section 5 we present numerical calculations of the wave propagation in active waveguides.

## 2. Characterization of Waves in Waveguides

Discussion of propagation of the optical field through *passive* waveguides is usually limited to the discussion of the guided waves, *i.e.* waves (modes) which are spatially confined in the waveguide core. In the *active* devices, however, the sources of photons are located inside the guiding layer and therefore the amount of energy coupled to the guided modes may be comparable or smaller than the energy coupled to other modes. On that account, all waves must be considered when dealing with active devices.

In this section, we review the general theory of planar (slab) waveguides.[18–20] We consider a structure with three layers[a] of a dielectric described by a (generally complex) refractive indices $n_1$ (cladding), $n_2$ (core) and $n_3$ (substrate), see Fig. 1b; we assume for the sake of clarity for the real parts of the refractive indices $n_2 > n_3 > n_1$. The thickness of the core $d$ is comparable with or larger than the vacuum wavelength of the optical radiation $\lambda$. The cladding and the substrate are optically thick and therefore considered to be infinite. The $z$ axis is the propagation axis and the $x$ axis is perpendicular to the waveguide layer.

Electromagnetic field from a source within a waveguide is coupled only to the states of a field which are allowed by boundary conditions — to the modes of the waveguide. According to the symmetry of the

[a] The structure with a step-like profile of the refractive index is taken into account for the sake of clarity. The theory may be, however, generalized to an arbitrary profile of refractive index including a continuous graded profile. Comparison of calculated PL spectra with our experimental data has been done considering the real parameters of our samples, *i.e.* graded profile of refractive index across the waveguide.

waveguide, the intensity of electric field of a TE mode may be written as $\vec{E}(x,z,t) = \hat{y}E(x,z)\mathrm{e}^{-\mathrm{i}\omega t}$, where $\hat{y}$ is a unit vector in the $y$ direction, $\omega = 2\pi c/\lambda$ is the frequency of the mode, $c$ is the light velocity and

$$E(x,z) = \{A_{m\beta}\exp[\alpha_{m\beta}(x-x_m)] + B_{m\beta}\exp[-\alpha_{m\beta}(x-x_m)]\}\mathrm{e}^{\mathrm{i}\beta z} \qquad (1)$$

in every layer denoted by the index $m$ ($m$=1,2,3). The modes are fully characterized by the propagation constant $\beta$, which may be interpreted in terms of the angle of propagation $\theta_2$ (see Fig. 1b) of a ray: $\beta = (2\pi n_2 \sin\theta_2)/\lambda$. A variable $\alpha_{m\beta} = [\beta^2 - (2\pi n_m/\lambda)^2]^{1/2}$ determines the profile of the mode in the $x$ direction, $x_m$ is a coordinate of the boundary between the $m$-th and ($m$+1)-st layer and the variables $A$ and $B$ are constants for every layer and mode, fully determined by the boundary conditions and normalization.[20] The axial system has been adapted by rotation in order to ensure $\vec{E} \parallel \hat{y}$. In our case of a three-layer structure, the modes may be resolved into three groups depending on their spatial profile in the direction of the $x$ axis, hence depending on the values of the coefficients $\alpha_{m\beta}$. Let us consider for instance a lossless structure, *i.e.* $n_m$ real. The maximum value of $\beta$ for propagating waves is clearly $2\pi n_2/\lambda$, therefore $\alpha_{2\beta}$ is always imaginary and the field intensity in the core is nonzero. Other $\alpha$'s, on the contrary, may be real or imaginary.

For both $\alpha_{1\beta}$ and $\alpha_{3\beta}$ imaginary, the mode takes the form of a propagating wave in all three layers and it is called the *radiation mode*. In terms of the ray optics, a ray emitted by a source inside the waveguide is refracted either to the substrate or to the cladding and only a small portion of its energy is reflected back to the core. The energy of the mode is therefore radiated from the waveguide core on short distances compared to the waveguide thickness $d$.

If the coefficients $\alpha_{1\beta}$ and $\alpha_{3\beta}$ are, on the contrary, both real, the profile of the mode in the cladding and the substrate given by Eq. (1) takes the form of evanescent waves and the mode energy is localized predominantly in the core. The mode is bound to the layer with the highest refractive index and propagates along the $z$ axis, and it is called the *guided mode*. In terms of the ray optics, a ray is incident on both boundaries core/cladding and core/substrate at an angle larger than the critical angle for total internal reflection, therefore it is totally reflected and its energy cannot leave the core. Near the critical propagation

constant $\beta_C = 2\pi n_3 / \lambda \leq \beta$, the coefficient $\alpha_{3\beta}$ is close to zero and thus the attenuation of the evanescent wave in the substrate is very weak and the wave penetrates into the substrate to depths comparable or even larger than the core thickness.[21]

*Substrate radiation modes*[b] *(substrate modes)* are the last kind of the waveguide modes. They are characterized by a real coefficient $\alpha_{1\beta}$ and an imaginary coefficient $\alpha_{3\beta}$. The wave may propagate in the substrate but it is totally reflected at the core/cladding boundary. The substrate modes are very similar to the radiation modes since the energy radiated by an emitting nanocrystal to that mode may leave the core on short distances in the $z$ direction, however the energy of the modes with the propagation constant near the critical propagation constant, *i.e.* $\beta \leq \beta_C$, may reside inside the core layer at large distances from the source, by orders of magnitude larger than the core thickness. The propagation angle $\theta_2$ of such mode is near the critical angle for total reflection on the core/substrate boundary, thus the reflectivity is slightly below 1 and only a small portion of energy is lost during one round-trip of the ray across the core layer (*cf.* Fig. 1b). The angle of propagation of the mode in the substrate is near $\pi/2$ implying that the mode propagates along the core/substrate boundary and in many experiments these modes cannot be distinguished from regular guided modes. Since the substrate modes propagate mostly outside the core, their characteristics are determined by the optical constants of the substrate. Nevertheless, the aforementioned substrate modes with $\beta \approx \beta_C$ are affected by the core properties near the source. Therefore they behave like guided modes at the distances smaller than a characteristic distance[18] of their leakage to the substrate but at the larger distances they behave more like free plane waves in the substrate.

[b] In our previous publications, substrate radiation modes have been inaccurately denoted as "leaky" waves or leaky modes. The label *leaky modes* should be rather reserved for a special sort of unphysical solutions of the wave equation with boundary conditions determined by the symmetry of a waveguide.[20]

## 3. Spectral Filtering of the Modes

In this section, we present a simple model which explains how the TE and TM modes are formed and which types of the waveguide modes take part in the spectral filtering process. We consider a large planar waveguide with the radiating nanocrystals uniformly distributed in the *yz* plane and therefore the system is assumed to have a full translational symmetry in both *y* and *z* directions. This model is therefore not able to simulate phenomena which arise from the wave propagation (for appropriate models, see sections 4 and 5) since the symmetry-breaking due to the sample edge is not included in the description, however the principle of the peak formation in the PL spectra is best illustrated.

The main idea of the model follows from the aforementioned fact that the substrate modes with the propagation constant slightly below the critical value undergo several round-trips in the core before their energy leaves the core. Due to the interference effects (similarly to the Fabry–Perot interferometer),[22] the nanocrystals couple effectively only to the resonant modes, *i.e.* to the modes whose phase is reconstructed after one round-trip. These modes, in addition, refract to the substrate under an angle near $\pi/2$, therefore they are hardly distinguishable from the guided modes in experiments and we observe a superposition of the guided and the substrate modes in the PL spectra. Using the detection system with a small numerical aperture,[2] substrate modes with a fixed propagation angle are selected (*cf.* Fig. 1b) and the resonances arise for certain wavelengths only. These resonances are then observed as sharp peaks in the PL spectra.

To give a more quantitative description, let us consider nanocrystals randomly oriented and randomly located in the waveguide core which radiate the optical field with intensity of electric field $E_0(\lambda)$ under an angle $\theta_2$. The total field at the position of the nanocrystal is evaluated as a sum of the field $E_0$, the field after one round-trip in the core, the field after two round-trips *etc.* Mathematically, we express the field as an infinite series:

$$E_{\text{internal}}(\lambda,\theta_2) = E_0(\lambda)\{1 + r_{21}r_{23}\exp[\mathrm{i}4\pi n_2 d\cos\theta_2/\lambda] + \\ + (r_{21}r_{23}\exp[\mathrm{i}4\pi n_2 d\cos\theta_2/\lambda])^2 + \ldots\} = \frac{E_0(\lambda)}{1 - r_{21}r_{23}\exp[\mathrm{i}4\pi n_2 d\cos\theta_2/\lambda]}, \quad (2)$$

where $r_{21}$ and $r_{23}$ represent the reflection coefficients at the core/cladding and the core/substrate boundaries, respectively, which depend upon the propagation angle $\theta_2$. Note that the summation is possible in lossless structures only if $|r_{21}r_{23}|<1$, therefore Eq. (2) is valid only for the radiation and the substrate modes, the guided modes (with $|r_{21}|=|r_{23}|=1$) will be discussed hereafter. Function $|E_{\text{internal}}(\lambda,\theta_2)|^2$ defined by Eq. (2) stands for light intensity in the core of the waveguide and has maxima at the resonances for the wavelengths $\lambda$ for which the condition $\mathrm{Im}(r_{21}r_{23}\exp[\mathrm{i}4\pi n_2 d\cos\theta_2/\lambda]) = 0$ is fulfilled.

### 3.1. *Substrate and radiation modes*

Considering only the substrate modes, $|r_{21}|=1$ and $|r_{23}|<1$. The more is the value $|r_{23}|$ close to unity, the narrower are the peaks in the intensity $|E_{\text{internal}}(\lambda)|^2$. Additionally, the peak value increases with increasing $|r_{23}|$ and thus the substrate modes are most visible for angles $\theta_2$ approaching the critical angle for total internal reflection on the core/substrate boundary. For radiation modes, the value $|r_{23}|$ is usually much less than unity and thus the spectra of the radiation modes reveal only broad peaks with a small peak-valley contrast.

In experiments, the detector has a nonzero numerical aperture and therefore radiation from a nonzero spatial angle is collected. The total intensity recorded by the detector is then

$$I_{\mathrm{S}}(\lambda,\alpha) = \int_{\alpha-\Delta\alpha/2}^{\alpha+\Delta\alpha/2} \left|E_{\text{internal}}(\lambda,\theta_2)\right|^2 T_{23}(\theta_2) T_{\mathrm{S}}(\alpha') \frac{\mathrm{d}\theta_2}{\mathrm{d}\alpha'} \mathrm{d}\alpha', \quad (3)$$

where the detection angle is given by its mean value $\alpha$ (*cf.* Figs. 1a-b) and $\Delta\alpha/2$ denotes the numerical aperture of the detector. The symbols $T_{23}$ and $T_{\mathrm{S}}$ stand for the respective transmittances at the core/substrate boundary and at the sample edge, which are given by the Fresnel formulae. The detection angle $\alpha'$ and the propagation angle $\theta_2$ are connected by the Snell's law

$$n_2^2 \sin^2 \theta_2 = n_3^2 - \sin^2 \alpha' . \tag{4}$$

The expression $\mathrm{d}\theta_2 / \mathrm{d}\alpha'$ in Eq. (3) stands for the angular mode density and reflects the fact that the nanocrystals radiate isotropically in the core.

### 3.2. *Guided modes*

For the guided modes, the field intensity $|E_0(\lambda)|^2$ in the core is enhanced similarly to Eq. (2), however losses due to radiation at the sample edge should be included in order to get a physically correct formula. Such derivation is beyond this simple model and therefore we consider that the intensity of the electric field is given by the formula

$$E_{\mathrm{guided}}(\lambda, \theta_2) = F(\lambda, \theta_2) E_0(\lambda), \tag{5}$$

with $F(\lambda,\theta_2)$ being the enhancement factor similar to the factor in Eq. (2). The detected intensity is

$$I_{\mathrm{G}}(\lambda, \alpha) = \int_{\alpha-\Delta\alpha/2}^{\alpha+\Delta\alpha/2} \mathrm{d}\alpha' \int_0^{\pi} \mathrm{d}\theta_2 \left| E_0(\lambda) F(\lambda, \theta_2) \right|^2 T_{\mathrm{G}}(\lambda, \theta_2) D_{\mathrm{G}}(\lambda, \theta_2, \alpha'), \tag{6}$$

where $T_{\mathrm{G}}(\lambda,\theta_2)$ stands for the transmittance of the mode denoted by its wavelength $\lambda$ and propagation angle $\theta_2$ through the sample edge and $D_G(\lambda,\theta_2,\alpha')$ is the diffraction efficiency from the mode to the diffraction angle $\alpha'$. The enhancement factor $F(\lambda,\theta_2)$ has sharp maxima, *i.e.* only the guided modes with well resolved propagation angle are allowed by the waveguide, therefore we may simplify[c] Eq. (6):

$$I_{\mathrm{G}}(\lambda, \alpha) = \int_{\alpha-\Delta\alpha/2}^{\alpha+\Delta\alpha/2} \left| E_0(\lambda) F(\lambda) \right|^2 T_{\mathrm{G}}(\lambda) D_{\mathrm{G}}(\lambda, \alpha') \mathrm{d}\alpha' . \tag{7}$$

Decoupling of electromagnetic waves from a dielectric waveguide to free space (evaluation of the functions $T_{\mathrm{G}}(\lambda)$ and $D_{\mathrm{G}}(\lambda,\alpha')$) cannot be described simply by the Snell's law but we must take into account diffraction and full boundary conditions. Such approach is, however, beyond the scope of this paper, therefore we assess the situation only qualitatively. It is well known that diffraction on a slit with aperture

[c] We consider here for the sake of simplicity one guided mode for all wavelengths, however Eq. (7) may be extended to a general case of multimode guiding.

width comparable to the light wavelength produces a wide diffraction maximum in the Fraunhoffer limit, thus we may conclude that the function $D_G(\lambda,\alpha')$ has a broad peak[16] in the second variable. The guided modes, unlike the substrate modes, cannot be distinguished one from the other by selecting the angle of detection.

The magnitude of the transmittance $T_G$ may be estimated from the Fresnel formulae; we assume that for the angle of incidence at the waveguide edge well above the critical value for the total internal reflection at the boundary the transmittance is low while for smaller angles, the modes are decoupled more effectively. Simple derivation gives that the guided modes near the cut-off wavelength are only weakly decoupled for $n_2^2 - n_3^2 > 1$. In waveguides where $n_2^2 - n_3^2 < 1$, all guided modes may be radiated from the waveguide core with high transmittance.

### 3.3. *All modes together, comparison with experiment*

The total intensity at the detector is

$$I(\lambda) = I_S(\lambda) + I_G(\lambda) + I_R(\lambda). \tag{8}$$

The symbol $I_R(\lambda)$ denotes the spectrum of the radiation modes which is almost flat and always less intense when compared to the spectrum of the substrate modes as seen from Eq. (2). Therefore it plays a minor role and hence it is not discussed from now on. The detected PL spectrum then consists of the two major components which compete with each other: the broad spectrum of the guided modes and the spectrum of the substrate modes with narrow peaks. Visibility of the respective components is determined by the numerical aperture of the detection system and mainly by the geometrical properties of the sample since these determine the strength of decoupling of the guided modes.

The spectra of the substrate modes reveal one more property which has not been discussed yet. The phase of the reflection coefficient $r_{23}$ in Eq. (2) does not vary with the incident angle $\theta_2$ when considering substrate and radiation modes, however the phase of the coefficient $r_{21}$ does change from 0 to $\pi$ in the region of substrate modes (see Fig. 3 in Ref. 17). The phase is, in addition, dependent upon the mode polarization and therefore the peaks of the TE and TM modes split in the PL spectra.

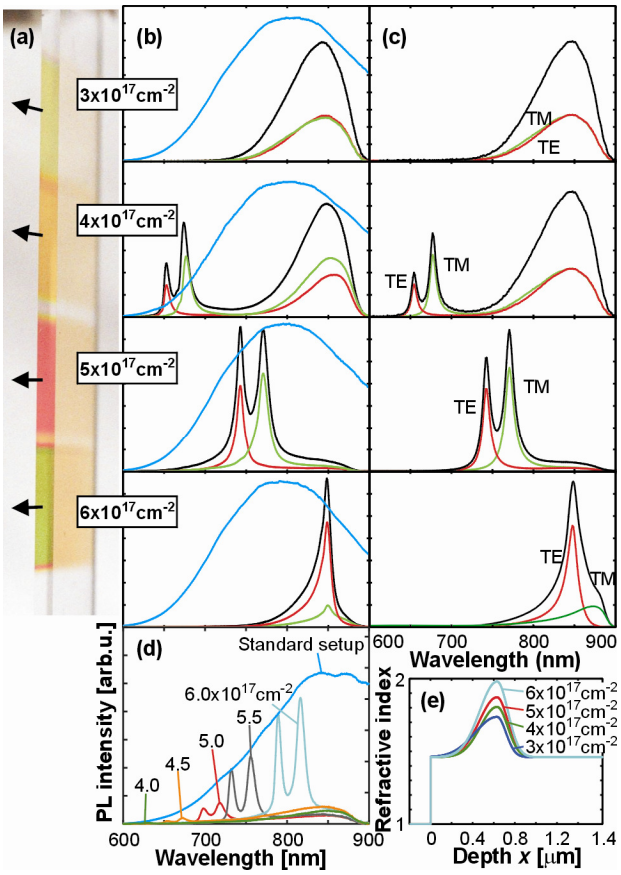


Fig. 2. (a) Photograph of the edge of a set of implanted layers with direction of PL indicated by arrows, the edge is on the left; (b) measured PL from samples implanted to different Si-ion fluences (indicated on the left) in standard (blue line) and waveguiding geometry (black line, red and green lines stand for TE and TM resolved polarizations); (c) theoretically calculated PL spectra; (d) comparison of PL measured in the waveguiding geometry for different series of implant fluences with the PL measured in the standard geometry (broad band); (e) profiles of refractive index of the samples with indicated implant fluences.[17]

Fig. 3. (a) Measured PL spectra with a drop of various liquids above the excitation spot; (b) theoretical PL spectra; (c) comparison of experimental (points) and theoretically calculated positions of PL maxima for different refractive indices of the liquids. The sample with an implant fluence of $5{\cdot}10^{17}$ cm$^{-2}$.[24]

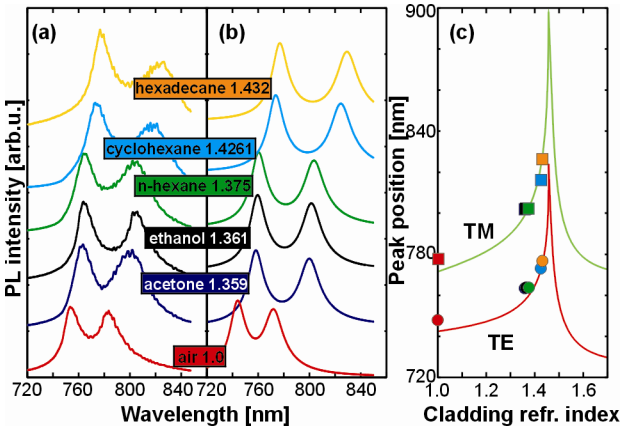

In the three-layer waveguides as discussed in this chapter, the TE mode peak is red-shifted with respect to the TM mode peak. The spectral positions of the peaks may merge or interchange in the waveguides with other profile of the refractive index.

We compared the predictions of our model with the PL spectra measured on samples prepared by $Si^+$ ion implantation (for details of the experimental set-up and sample preparation, see Refs. 2, 8 and 17). With the help of near-IR transmission measurement and the SRIM software,[23] we obtained the refractive index profiles of our waveguides (see Fig. 2e) which were then used in numerical simulations. The samples with higher implant fluences reveal higher peak values of the refractive index. The experimental spectra are shown in Fig. 2b and our theoretical simulations in Fig. 2c. Fig. 2d shows the PL spectra from another series of samples implanted to different fluences where the scaling of the narrow peak intensities can be clearly seen — the peak magnitudes follow well the spectral course of PL of free nanocrystals (PL measured in the standard setup).

The experimental data in Fig. 2b reveal significant modulation of the PL spectra when detecting in the waveguiding geometry. In the standard geometry (blue line), only the broad PL spectrum characteristic of Si nanocrystals is displayed and its shape is almost independent of the density of nanocrystals. Measurements in the waveguiding geometry, on the contrary, reveal the two abovementioned distinct linearly polarized peaks (black line without resolution of polarization, red and green lines represent TE and TM polarization, respectively) which move to longer wavelengths with increasing density of nanocrystals, and a broader peak centred around 850 nm which is unpolarized and its spectral position remains the same in all samples. The broad peak is interpreted as the spectrum of the guided modes: for the lowest concentration of nanocrystals (implant fluence of $3\times10^{17}$ $cm^{-1}$), our calculations show that the cut-off wavelengths are below 600 nm and above 1.5 μm and thus the substrate modes are missing in the selected spectral region. The interpretation is supported by the fact that the broad peak is not polarized, its shape and magnitude are only weakly dependent on nanocrystal density (Fig. 2d) and its spectrum is similar to the spectrum measured in the standard geometry (absorption cuts the spectrum of the

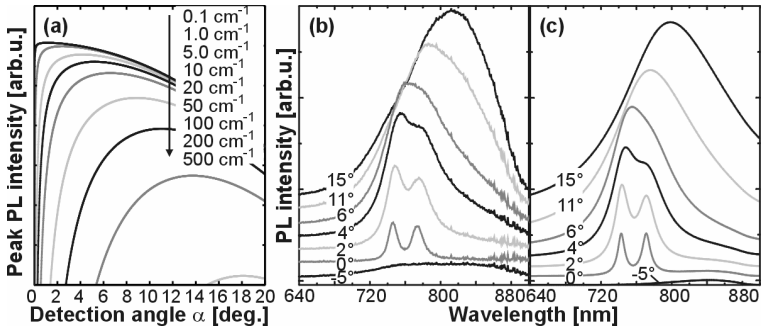


Fig. 4. (a) Theoretical dependence of peak PL intensity on the angle of detection $\alpha$ for various absorption coefficients of the core; (b) measured PL spectra at different detection angles; (c) numerical simulations of the measurements. The sample with an implant fluence of $5\times10^{17}$ cm$^{-2}$.

guided modes below 750 nm). The substrate modes are not influenced by the absorption since they propagate mostly in the transparent substrate.

According to Eq. (8) and the subsequent discussion, the theoretical spectra represent the sum of the contributions from the two types of the modes. We are not able to determine the spectrum of the guided modes analytically within this model and thus we treat the experimental PL spectrum from the sample with the lowest nanocrystal density as the spectrum of the guided modes in all samples. The spectra of the substrate modes are then calculated according to Eq. (3) and added to the spectrum of the guided modes. Comparison of the resulting theoretical spectra in Fig. 2c to the experimental data in Fig. 2b gives an excellent agreement indicating a good precision of our model.

In experiments, we are able to set the detection angle $\alpha$ or the numerical aperture of the detector, therefore the angular properties of the PL should be discussed. The angle of detection may influence the detected spectra in two distinct ways: (1) magnitude of the photoluminescence and (2) shape of the spectra. The spectrum of the guided modes changes with the angle of detection only slightly,[16] therefore we discuss here only the substrate modes which reveal the most significant changes. The variance of the peak magnitude of the spectra may be evaluated directly from Eq. (3) considering $|E_0(\lambda)| = \text{const.}$ and considering exact resonance, *i.e.* $\mathrm{Im}\{r_{21}r_{23}\exp[\mathrm{i}4\pi n_2 d\cos\theta_2/\lambda]\} = 0$ — it is plotted in Fig. 4a for several absorption coefficients of the core

material taken at the wavelength of 500 nm. The peak position of the PL magnitude is not constant and shifts towards the larger values of the detection angle with increasing absorption coefficient. Besides the overall intensity, the PL spectra change also in shape when the angle $\alpha$ is varied as seen in our experimental results depicted in Fig. 4b. With increasing angle $\alpha$, the peaks broaden and shift towards longer wavelengths. The interpretation is straightforward within our model: increase of the angle $\alpha$ implies decrease of the angle $\theta_2$ and therefore decrease of the reflection coefficient $r_{23}$ and, in addition, change of the phase of the reflection coefficient $r_{21}$. The former is responsible for the peak broadening while the latter causes a change of the phase matching condition and thus the spectral shift of the peaks. Our theoretical simulations in Fig. 4c agree with the experimental results in Fig. 4b which indicates correct interpretation and modelling. We feel that these experiments with detection at different angles can be hardly interpreted in terms of delocalized guided modes since there is no reason for the guided modes to reveal markedly different spectra in different diffraction directions.

### 3.4. *Differentiation of the substrate modes from the guided modes*

In order to support experimentally our model, we performed a novel experiment published in Refs. 17 and 24. The refractive index of the cladding layer may be easily modulated for example by dropping a small volume of liquid onto the sample. If the refractive index of the whole layer is changed, the PL spectra should change due to the obvious change of the phase of the reflection coefficient $r_{21}$. The measured spectra for the sample implanted to the fluence of $5\times10^{17}$ cm$^{-2}$ are depicted in Fig. 3a and our numerical simulations in Fig. 3b. The theoretically estimated dependence of the peak positions and their comparison to the experiments are the plotted in Fig. 3c. The guided and the substrate modes may be then unambiguously resolved if a small drop of the liquid is placed only between the excitation spot and the sample edge. The modes with their characteristic spectra form within a short distance from the excitation spot where the waveguide is not modified by the liquid. The guided modes then pass through a modified waveguide where the

cut-off frequency and thus the resonance condition for the delocalized modes are shifted. If the model based on delocalized guided modes were valid, we would thus expect a shift of the spectral positions of the peaks. The substrate modes, on the contrary, are already decoupled from the core at the position of the liquid and propagate freely in the substrate and therefore the core/cladding boundary cannot influence them. The PL spectra are then, in the case of validity of our model of substrate modes, expected to remain unchanged when compared to the original spectra without any liquid above the sample. The experimental data[17] prove the correctness of the concept of the substrate modes since the spectra do not modify when dropping a liquid between the excitation spot and the edge.

Obviously the active waveguides may be used as sensitive detectors of refractive index changes (we estimate their sensitivity up to $10^{-5}$) which may be tuned for particular applications via tailoring the preparation parameters as shown in Ref. 25. The spectral region in which the detector may work is not limited only to the PL band of nanocrystalline silicon as shown experimentally in Ref. 14. The data presented therein show that light with a broad spectrum may be coupled to the substrate modes from outside. The modes which fulfil the resonance condition are then absorbed in the core and the reflection reveal dips at the theoretical spectral positions of the PL peaks, which is in agreement with our model.

## 4. Wave Propagation in Waveguides

In this section, we introduce an advanced model capable of describing the wave propagation in the direction along the waveguide layer. Within this theory, we are able to interpret the mechanism of the mode formation and we may evaluate the influence of the net optical gain or losses on the PL intensity. Although the model is formulated in terms of the ray optics (and an approximative description of the wave propagation), it gives good qualitative predictions and it is helpful when interpreting the experiments. A more subtle but with difficulty interpretable model usable for quantitative predictions is introduced in section 5.

Since we are interested here in wave propagation, we must take into consideration the fact that nanocrystals emit generally spherical waves and thus the signal recorded by a spatially limited detector decreases with the distance from the source as already discussed in Ref. 26 for a special case. The real detector collects the signal from a nonzero spatial angle as well as the input aperture has a nonzero spatial area and therefore there are two limiting cases for which we develop our theory: (1) A small detector with a large numerical aperture (NA), typically an optical fibre capable of high spatial resolution and small angular resolution, and (2) A detector with a small NA thus with a high angular resolution. Since the energy density of a spherical wave decreases as $1/r^2$, where $r$ denotes a distance from a source, the intensity detected in the case 1 by a spatially small detector also decreases as $1/r^2$. In the latter case, on the contrary, when the characteristic size of the input lens of the detector is much larger than $r$, the signal would be independent of the distance from the source. We therefore denote the coupling coefficient as $\rho(\zeta)$ in the following text for spherical waves, *i.e.* for the case 1. The positive variable $\zeta = -z_N$ denotes the distance between the excited spot and the sample edge, $z_N$ being the position of the excited spot at the axis $z$. For detectors with a small NA and high angular resolution, we put $\rho(\zeta)=1$.

We divide the initial discussion into the guided and the substrate modes while the radiation modes are omitted for the sake of simplification (as discussed above, they play only a minor role).

### 4.1. *Guided modes*

It was stated above in section 3 that the PL from Si nanocrystals couples to the guided modes in the whole spectral region and that the spectrum of the guided modes is nearly equal to the spectrum of the PL of the unperturbed nanocrystals.[d] A wave emitted by a nanocrystal at a distance $\zeta$ from the sample edge is amplified or attenuated depending on the gain

[d] The spectral intensity of the modes is proportional to the number of the guided modes. Therefore the spectral intensity of the light carried out by the modes may reveal jumps at distinct wavelengths which correspond to the cut-off wavelengths.

and the loss coefficients, and the intensity transmitted through the edge takes the form (according to Eq. (6))

$$I_{\mathrm{G},2}(\lambda,\alpha,\zeta)=I_0(\lambda)\left|F(\lambda)\right|^2\rho_{\mathrm{G}}(\zeta)\exp\left[\left(g(\lambda)-\gamma(\lambda)\right)\zeta\right]\times \\ \times\int_{\alpha-\Delta\alpha/2}^{\alpha+\Delta\alpha/2}T_{\mathrm{G}}(\lambda,\theta_2)D_{\mathrm{G}}(\lambda,\theta_2,\alpha')\mathrm{d}\alpha', \tag{9}$$

where $g(\lambda)$ and $\gamma(\lambda)$ stand for the gain and the loss coefficient, respectively, $I_0(\lambda)=|E_0(\lambda)|^2$ is the spectral intensity of the PL and $\rho_{\mathrm{G}}(\zeta)$ is the coupling coefficient. The dependence of the gain and the loss coefficients on wavelength reflects only properties of the material (the role of mode delocalization is neglected since our calculations show it is small) and we consider in the following that the major portion of the energy of guided modes is localized inside the core.

The coupling coefficient cannot be expressed simply as $1/\zeta$ since the detector is outside the waveguide core and the wave refraction at the sample edge, illustrated in Fig. 1c, is responsible for a slight modification. Considering only rays near the normal incidence in Fig. 1c, the intensity radiated to the angle $\phi_2$ is $I_0\phi_2/2\pi$. After refraction, this energy further propagates in the *yz* plane with divergence given by an angle $\phi_0=n_2\phi_2$ and at the position of the detector (its distance from the sample edge being $D$), the energy is spread over the arc with length $\phi_2(n_2D+\zeta)$. In the *xz* plane, the wave decoupled from the waveguide is also divergent, however the distance $D$ is fixed and the divergence contributes to the coupling coefficient by a constant term $1/D$. It is then easy to express the coupling coefficient for the guided modes as

$$\rho_{\mathrm{G}}(\zeta)=\frac{1}{n_2D+\zeta}. \tag{10}$$

Note that this formula is valid only for the spatially small detector, for a large detector with small NA we should write $\rho_{\mathrm{G}}(\zeta)=1$.

### 4.2. *Substrate modes*

Unlike the guided modes, where we usually cannot resolve the particular guided modes by the angle of detection and the PL spectrum is similar to

the PL spectrum of unperturbed nanocrystals, the substrate modes reveal maxima and minima in the spectra according to the constructive or destructive interference, respectively. The shape of the spectra depends on the number of internal reflections in the core and thus on the distance which the mode propagates. To express the shape of the spectrum mathematically, we then modify Eq. (3) in order to account for the coupling and Eq. (2) must be adapted to the finite number of reflections. The intensity emitted from the substrate then reads

$$I_{\mathrm{S},3}(\lambda,\alpha,\zeta)=\rho_{\mathrm{S}}(\theta_2,\zeta)\int_{\alpha-\Delta\alpha/2}^{\alpha+\Delta\alpha/2}\left|E_{\mathrm{internal}}(\lambda,\theta_2,\zeta)\right|^2 T_{23}(\theta_2)T_{\mathrm{S}}(\alpha')\frac{\mathrm{d}\theta_2}{\mathrm{d}\alpha'}\mathrm{d}\alpha', \quad (11)$$

where

$$\left|E_{\mathrm{internal}}(\lambda,\theta_2,\zeta)\right|^2=\left|\frac{1-[P(\lambda,\theta_2)]^{N(\theta_2,\zeta)+1}}{1-P(\lambda,\theta_2)}\right|^2 I_0(\lambda), \quad (12)$$

$$P(\lambda,\theta_2)=r_{21}(\theta_2)r_{23}(\theta_2)\exp[(g(\lambda)-\gamma(\lambda))z_{\mathrm{R}}/2]\exp[\mathrm{i}4\pi n_2 d\cos\theta_2/\lambda]. \quad (13)$$

Here $N(\theta_2,\zeta)$ is the number of reflections of the wave inside the core and $z_{\mathrm{R}}$ is the distance between two points of reflection on the core/substrate boundary (see Fig. 1b). The intensity of radiation which remains in the core may be expressed by a formula similar to Eq. (9), however we account for the wave leaking by the effective attenuation coefficient $\gamma_{\mathrm{eff}}$:[18]

$$I_{\mathrm{S},2}(\lambda,\alpha,\zeta)=I_0(\lambda)\rho_{\mathrm{G}}(\zeta)\exp[(g(\lambda)-\gamma(\lambda)-2\gamma_{\mathrm{eff}}(\lambda,\theta_2))\zeta]\times \int_{\alpha-\Delta\alpha/2}^{\alpha+\Delta\alpha/2} T_{\mathrm{G}}(\lambda,\theta_2)D_{\mathrm{G}}(\lambda,\theta_2,\alpha')\mathrm{d}\alpha'. \quad (14)$$

In order to evaluate *N*, we consider that after *N* reflections of a ray on the core/substrate boundary (see Fig. 1b) the intensity in the core with $g=\gamma=0$ may be expressed as $I_{\mathrm{S},2}(N,\zeta)=I_0\left|r_{21}r_{23}\right|^{2N}=I_0\exp[-2\gamma_{\mathrm{eff}}\zeta]$. The number of reflections may be then evaluated in the following way:

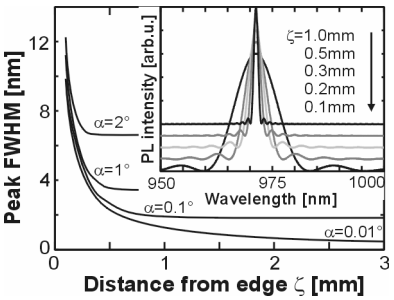


Fig. 5. Calculated dependence of the PL peak width on the length of propagation of the substrate mode for several angles of detection; inset: spectral profiles of PL for $\alpha$=1°.[25]

$$N = -\gamma_{\text{eff}}\,\zeta / \ln\left|r_{21}r_{23}\right|, \tag{15}$$

$$z_{\text{R}} = -\ln\left|r_{21}r_{23}\right| / \gamma_{\text{eff}}\,. \tag{16}$$

The effective attenuation coefficient may be calculated from the Poynting vector.[18] In the case of an asymmetric waveguide with the step-like profile of the refractive index, the coefficient may be expressed for TE waves as

$$\gamma_{\text{eff}} = -\mathrm{i}\frac{{\alpha_{2\beta}}^2}{\beta d}\frac{\alpha_{3\beta}}{\left(\alpha_{2\beta}+\alpha_{3\beta}\right)^2}, \tag{17}$$

with $\alpha_{2,3\beta}$ defined in section 2 and $\beta$=2π$n_2$sin$\theta_2/\lambda$. In structures with more complicated profile of the refractive index, the attenuation coefficient and the reflection coefficients must be evaluated numerically, however Eqs. (13) to (16) remain valid. The coupling coefficient may be, after simplifications and considering $\theta_2$ near the critical angle $\theta_{\text{C}}$, evaluated from the geometry of the system as

$$\rho_S\left(\theta_2,\zeta\right) = \left[\sqrt{2\frac{\theta_C-\theta_2}{n_3}\sqrt{n_2^2-n_3^2}\left(\zeta+n_2D\right)\left(\zeta+n_3D\right)}\right]^{-1}. \tag{18}$$

The PL spectrum of the modes radiated to the substrate obviously reveals narrow peaks for sufficiently large number of reflections, *i.e.* after a sufficiently long propagation of the mode. The modes which are excited near the sample edge undergo only several reflections and their spectrum is almost flat. With the increasing propagation length, the resonances become better resolved and the spectrum gets narrower as shown in

Fig. 5 where we plot the results of the numerical evaluation of Eqs. (11)-(13) for the special case of a step-like profile of the refractive index. For different profiles, the modes may form at distances differing by orders of magnitude as seen when comparing *e.g.* Refs. 10 and 27.

### 4.3. *Optical gain*

Our aim in this paragraph is to discover the role of the optical gain in waveguiding samples. Let us consider the VSL measurement of the net optical gain: a stripe of the length $\ell$ is optically excited and we detect the total light intensity radiated from the sample in the waveguiding setup. The PL comes from all excited nanocrystals in the stripe and thus the total ASE intensity may be expressed as an integral of Eqs. (9), (11) and (14):

$$I_{\mathrm{ASE}}(\lambda,\alpha)=\int_0^{\ell}\left[I_{\mathrm{G},2}(\lambda,\alpha,\zeta)+I_{\mathrm{S},2}(\lambda,\alpha,\zeta)+I_{\mathrm{S},3}(\lambda,\alpha,\zeta)\right]\mathrm{d}\zeta\,. \quad (19)$$

The above formula is composed of the respective contributions from the guided modes, the substrate modes diffracted from the core and the substrate modes refracted from the substrate. The three contributions have generally different magnitudes because of different mechanisms of decoupling of the associated waves at the sample edge. Since the efficiencies of the wave decoupling and the enhancement factor of the guided modes (see Eq. (7)) are unknown and depend on the particular sample geometry, we separate phenomenologically our discussion into two general cases: 1. majority of the guided modes (substrate modes cannot be distinguished in PL spectra) and 2. majority of the substrate modes.

1. If the *guided modes are dominant*, the energy of the radiating dipole in a silicon nanocrystal is coupled mainly to the guided modes. We may therefore neglect the contributions from the substrate modes and evaluate only the integral of Eq. (9). For the detector with a very small numerical aperture (*i.e.* when detecting plane waves, $\rho=1$), the integration yields the well known formula[15]

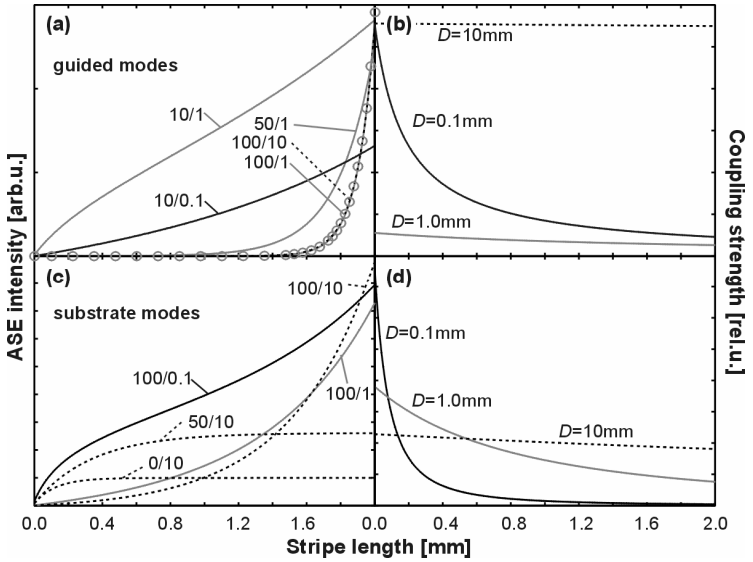


Fig. 6. Calculated ASE intensity from Eq. (19) as a function of the excited stripe length for the guided (a) and the substrate (c) modes; a small detector with a large NA is supposed. Coupling coefficients are plotted for comparison for the guided (b) and the substrate (d) modes. Scales of the curves are set for better comparison of their behavior. Numbers in (a) and (c) mean (gain coefficient in $cm^{-1}$)/(distance D between the sample and the detector in mm). Circles in (a) denote ASE intensity according to Eq. (20) with $(g-\gamma)=100\ cm^{-1}$.

$$I_{\mathrm{ASE}}(\ell) \propto \frac{\exp[(g-\gamma)\ell]-1}{g-\gamma}, \tag{20}$$

where $(g-\gamma)$ denotes the net gain. The result for a spatially small detector with a large NA obviously differs, however the result is not analytically integrable. We thus give only the numerical results in Fig. 6a — we compare evaluated Eq. (20) with Eq. (19) for the guided modes and the small detector for several values of the gain coefficient and the position of the detector. In order to give a clear interpretation of the graph, we plot in Fig. 6b the strength of coupling $\rho(\zeta)$ of the excited elements to the detector (the strength of coupling may be directly measured in the Shifting Excitation Spot[2] experiment (SES)). It is obvious from Figures 6a and 6b that Eq. (20) is valid only in special cases of the detection of plane waves by a spatially large detector or by a small detector at the

distance from the sample edge much larger than the length of the excited stripe. In the latter case, however, we may expect experimental complications because of the low PL intensity.

2. If the *substrate modes are dominant*, we consider that we detect ASE emission at the wavelength of one of the modes because at other wavelengths the contribution due to the substrate modes is negligible as discussed above and then the ASE intensity is modelled according to the discussion in the previous paragraph. The dominance of the substrate modes is caused by inefficient decoupling of the waves from the core at the sample edge and thus the major contribution comes only from the third term in Eq. (19). We plot in Figs. 6c-d the ASE intensity and the magnitudes of the coupling coefficient for several values of the gain coefficient and of the distance of the detector from the sample edge. The curves obviously show that Eq. (20) cannot be used for evaluation of the net gain in this case. For clear resolution of the net gain, one should use the SES method.

The theory developed in this section fits very well our experimental observations in VSL experiments. By choosing proper wavelength, we are able to select whether we detect guided or substrate modes and then we can directly compare their characteristics in one sample. An instructive result published in Ref. 28 means that the guided modes are more effectively amplified in the presence of a positive net optical gain than the substrate modes, as follows from the theory. We are also able to explain the unusual behaviour of the ASE and SES curves presented in Figs. 1e-f. The SES curve in Fig. 1f for the guided mode at 825 nm decreases monotoneously as the coupling coefficient decreases. The curves for the substrate TE and TM modes, however, initially increase and for longer distance of the excited spot from the edge they start to decrease due to the decrease of the coupling coefficient. The initial increase follows from the initial refraction of the waves into the substrate — since energy is radiated to the core and we detect the waves from the substrate, there is a nonzero propagation length necessary for leakage of the energy from the core. The position at which the SES curve reaches its peak depends on the detection angle (numerical aperture of the detector) as shown experimentally in Ref. 8 and as may be shown using our model.

## 5. Numerical Analysis of the Modes

Both models presented above are based on assumptions which simplify either the real geometry of the problem (consideration of the infinite waveguide in section 3) or the level of physical description (simple use of rays in section 4). In this section, we present a rigorous model which correctly describes propagation of the optical waves along the waveguide. The calculations in this section are performed numerically because it is impossible to derive the final expressions analytically.

The structure under description has three layers, two of them being infinite (the cladding and the substrate). According to the discussion in Ref. 20, the mode spectrum is then composed of discrete guided modes and the continuum of the substrate and the radiation modes. Presence of the continuum represents an unwanted feature in the numerical evaluation and therefore we overcome this problem by considering that all the layers are finite and the top and the bottom of the whole guiding structure is covered by a medium with reflectivity $r$=1. The waves propagate in the $z$ direction and we consider the edge at the coordinate $z$=0. We assume the infinite structure in the $y$ direction and we consider detection of the signal in the limit of Fraunhoffer diffraction (propagation of "plane" waves). The thickness of the cladding and the substrate is set to 0.6 mm, thus the angular resolution of the pattern diffracted from the edge is resolved with precision better than 0.15°.

The spatial profile of the intensity of electric field is given by Eq. (1) for TE modes, *i.e.* for the waves whose vector of electric intensity lies in the $y$ direction — the numerical analysis is performed only for the TE waves since the mode splitting is well explained by the simplified models and TM modes reveal similar behaviour to TE ones in other characteristics. Using the theory of Ref. 20, the calculations have been performed in the way briefly summarized in the following. First, the allowed propagation modes (*i.e.* modes with $\mathrm{Re}\,\beta > 0$) were found numerically — let us assume that the 2×2 transfer matrix for the whole structure without mirrors is $T_\beta$ and the relation between the field coefficients at the two opposite boundaries of the structure is[e]

[e] The medium with index 0 is an infinitesimally thin layer at the top of the cladding with refractive index $n_0$=$n_1$,

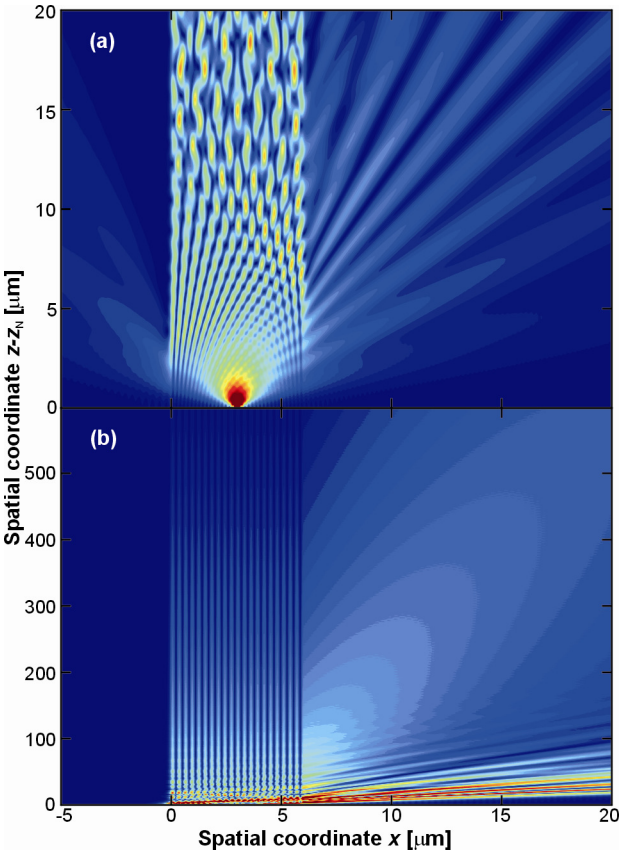


Fig. 7. (a) Distribution of the light intensity at wavelength 624.4 nm in the sample with 6 μm thick core; all modes are plotted. The coordinate $x$ means depth below the sample surface. (b) Detailed view of decoupling of the lowest–order substrate mode at long propagation distances; only substrate modes are plotted for clarity. Dark blue colour denotes minimum intensity, maximum intensity is dark red.

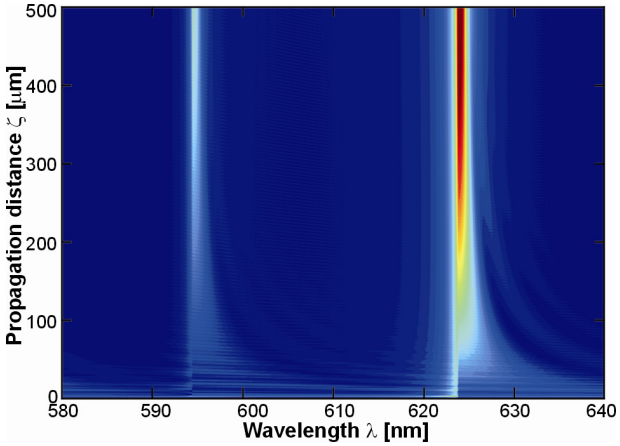


Fig. 8. Dependence of the light intensity on wavelength (horizontal axis) and propagation distance of the substrate modes (vertical axis). The waveguide has a core 6 μm thick.

$$\begin{pmatrix} A_{3\beta} \\ B_{3\beta} \end{pmatrix} = T_{\beta} \begin{pmatrix} A_{0\beta} \\ B_{0\beta} \end{pmatrix}. \tag{21}$$

Boundary conditions imply $A_{0\beta}=B_{0\beta}$ and $A_{3\beta}=B_{3\beta}$ and the (generally complex) coefficients $\beta$ which fulfil the above constraints were found iteratively. The second step consisted in calculation of the field distribution at the sample edge. We consider a nanocrystal at the coordinates $(x_{\mathrm{N}}, z_{\mathrm{N}} = -\zeta)$ which is coupled to the waveguide modes. The field $E_{\mathrm{rad}}(x,z_{\mathrm{N}})$ radiated by the nanocrystal may be decomposed to the modes as follows:

$$E_{\mathrm{rad}}(x, z_{\mathrm{N}}) = \sum_m \frac{[E_{\beta_m}(x', z_{\mathrm{N}}), \delta(x' - x_{\mathrm{N}})]}{\sqrt{[E_{\beta_m}(x', z_{\mathrm{N}}), E_{\beta_m}(x', z_{\mathrm{N}})]}} E_{\beta_m}(x, z_{\mathrm{N}}), \tag{22}$$

where $[\cdot,\cdot]$ stands for a scalar product (integral over the $x$ coordinate) and the summation goes over all allowed propagating modes. The field distribution at the sample edge is then, according to the propagating factor in Eq. (1), expressed as

$$E_{\mathrm{rad}}(x, z = 0) = \sum_m \frac{[E_{\beta_m}(x', z_{\mathrm{N}}), \delta(x' - x_{\mathrm{N}})]}{\sqrt{[E_{\beta_m}(x', z_{\mathrm{N}}), E_{\beta_m}(x', z_{\mathrm{N}})]}} E_{\beta_m}(x, z_{\mathrm{N}}) \exp[-i\beta_m z_{\mathrm{N}}]. \tag{23}$$

In the third step, we calculated the field diffracted from the sample edge in the Fraunhoffer limit by performing the Fourier transform on the function $E_{\mathrm{rad}}(x,z=0)$ and considering field refraction according to Snell's law and Fresnel formulae for simplification.

In the numerical results presented below, we consider a model system with the cladding with refractive index $n_1$=1 and width $w_1$ = 600 μm, the substrate with refractive index $n_3$ = 1.46 and width $w_3$ = 600 μm and the core has refractive index $n_2$ = 1.8 and its width is $d$ = 6 μm. Formation and propagation of the modes is illustrated in Figures 7a and 7b where we plotted the distribution of the light intensity in the structure (the coordinate $x$ = 0 refers to the core/cladding boundary). The beams which leave the core to the right are the substrate modes — we may assign an angle of propagation to each of them. It is interesting that obviously they are not radiated from the core at one distinct point but they decouple over long distances. This property is better visualized in the detailed view in Fig. 7b where we may identify the substrate modes which are rapidly

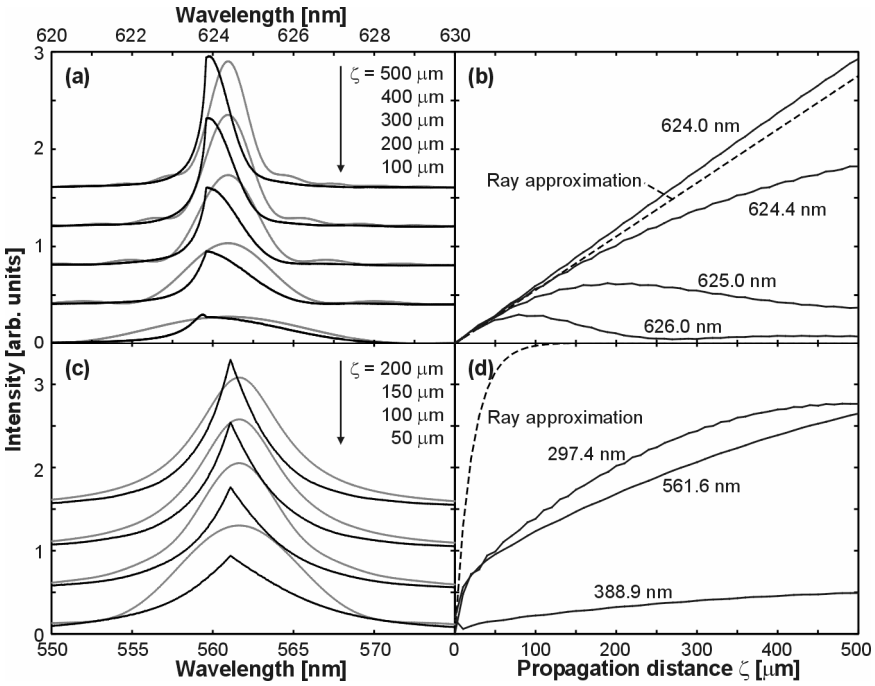


Fig. 9. (a), (c) Narrowing of the substrate mode during propagation along the waveguide. Spectral profiles of the modes at several distances from the excited spot calculated by the numerical model (black lines) and results of the ray model for comparison (gray lines). (b), (d) Calculated energy decoupled from the core as a function of the propagation distance from the excited spot (solid) and results of the ray model for comparison (dashed line). Parameters of the curves denote wavelengths in the vicinity of the resonance of the mode (b) and wavelengths of several resonant modes (d). The core thicknes is 6 μm (a), (c) and 0.6 μm (b), (d), respectively.

decoupled from the core and one mode which decouples at much longer distances comparable to 0.5 mm.

The results depicted in Fig. 7 directly support the model from section 4 based on the assumption of the gradual decoupling of the waves from the core to the substrate. As we have shown, this fact is responsible for gradual narrowing of the PL spectra when increasing $|z_N|=\zeta$, *i.e.* when the excited spot is moved further from the sample edge. We performed calculations in order to confirm this hypothesis and the results are plotted in Fig. 8 — the dependence of the PL intensity measured at the angle $\alpha$=2.5° on wavelength $\lambda$ and distance $|z_N|=\zeta$ between the nanocrystal and

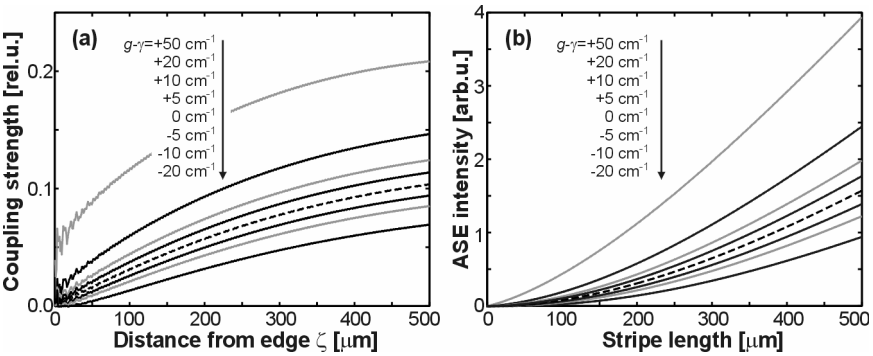


Fig. 10. (a) Calculated coupling strength of the excited spot at the distance $\zeta$ from the sample edge considering a sample with the core thickness of 6 μm for several values of gain coefficient at the resonant wavelength 624.4 nm of the substrate mode (*cf.* Figs. 7, 8); (b) calculated ASE intensity recorded from the sample with same parameters as in (a).

the sample edge. The cuts of this graph in the directions of both axes $\zeta$, $\lambda$ are plotted in Figures 9a and 9b. In Fig. 9a, the mode narrowing is obvious and we compare these numerical results with the results of the model from section 4 (plotted as grey lines). We may conclude that the approximate model gives accurate results and is therefore usable as an estimate for practical use in evaluation of experiments. The rate of energy decoupling from the core is depicted in Fig. 9b for several wavelengths around the resonance together with the estimate performed according to Ref. 18. Decoupling rate is obviously well estimated by the theoretical curve for the resonant mode and thus the ray model is usable also in this case. Graphs similar to those in Figures 9a and 9b are plotted in Figures 9c and 9d for the waveguide core with thickness of 0.6 μm together with comparison with the simplified model. The energy flow from the core to the substrate is more pronounced when compared to the waveguide with the wider core. We may interpret this feature in terms of ray propagation: as seen from Eqs. (16) and (17), the distance $z_R$ between the two points of reflection of the ray is proportional to the waveguide thickness and therefore the energy loss due to transmission to the substrate is faster in thin waveguides. Although qualitative discussion well reflects the situation, quantitative comparison in Fig. 9d fails. The limitations of the ray model from section 4 are thus clearly seen — it gives good numerical predictions only when $d>>\lambda$, *i.e.* when wave

propagation is well described by ray optics. The narrowing of the modes, nevertheless, may be roughly estimated by using the ray model also for structures with $d \sim \lambda$ as seen in Fig. 9c.

We may include small optical losses or optical gain (up to tens $cm^{-1}$) into the numerical model in the form of a complex refractive index. We present in Fig. 10a the dependence of the intensity of light emitted by a nanocrystal and transmitted through the structure with gain or losses on the distance of propagation. The detection angle is $\alpha = 2.5°$, wavelength 624.4 nm and other parameters equal to those in Fig. 7. By integration of the curves in Fig. 10a, we get the ASE intensity depicted in Fig. 10b. According to section 4, all the ASE curves seem to have exponential behaviour near the origin $\zeta = |z_N| = 0$, however this is not a consequence of the optical gain but the result of the mode leaking.

We may conclude this section by stating that the approximate models are capable of a qualitative description of the mode propagation and leaking in the waveguiding structures. They give good quantitative results if the waveguide core is wide enough ($d >> \lambda$) but one should use them only as rough estimates in other cases where numerical calculation should be applied in order to get quantitatively correct results.

## 6. Conclusions and Acknowledgements

The results presented in this chapter show that the substrate modes, usually considered as an unwanted artificial feature, have properties very different from the guided modes of the waveguide. Because of their limited lifetime inside the core, they cannot be effectively absorbed or amplified and therefore they are hardly controllable. In spectroscopic measurements, it appears almost impossible to evaluate the magnitude of the net optical gain from the VSL measurements on the substrate modes and therefore it is desirable to avoid (by properly designing the core parameters) the presence of the substrate modes in most applications including optical spectroscopy. The spatial separation of the substrate and the guided modes can be exploited in order to filter out the substrate modes, *e.g.* by using a detection with high spatial resolution or using techniques for decoupling of the guided waves from the core (by placing a prism on the top plane of the sample *etc.*).

The substrate modes may be, however, of importance in nano-silicon active optoelectronic devices where light is emitted, guided or amplified. Because of usual small optical gain in Si nanocrystals, the intensity of the substrate modes may be comparable to or even larger than the intensity of the guided modes and they may be then a source of noise. Devices must be then constructed in order to avoid wave propagation in the substrate — one may use for example absorbing substrate or a special geometry of the device in order to physically block the waves.

Although the substrate modes represent in most cases a parasitic feature in waveguiding devices, it appears, however, possible to use them in a wide range of applications in nano–optics. They may be used for optical sensing profiting from their sensitivity to the refractive index of the cladding. Another promising application may be the use of active waveguides as simple tunable sources of narrow–line directional optical emission and as tunable optical filters. However, further research in this direction is needed.

Financial support through research projects GAAVCR IAA1010316, GACR 202/01/D030, GACR 202/07/0818, Centrum LC510 and the institutional research plan AV0Z 10100521 (Institute of Physics) is greatly appreciated. This work is also a part of the research plan MSM 0021620834 that is financed by the Ministry of Education of the Czech Republic. Thanks are also due to Prof. R.G. Elliman (ANU Canberra) for kindly supplying samples used throughout this study.

## References

1. L. Pavesi, L. Dal Negro, C. Mazzoleni, G. Franzo and F. Priolo, *Nature* **408**, 440 (2000).
2. J. Valenta, I. Pelant and J. Linnros, *Appl. Phys. Lett.* **81**, 1396 (2002).
3. L. Dal Negro, M. Cazzanelli, L. Pavesi, D. Pacifici, G. Franzo, F. Priolo and F. Iacona, *Appl. Phys. Lett.* **82**, 4636 (2003).
4. L. Khriachtchev, M. Räsänen, S. Novikov and J. Sinkkonen, *Appl. Phys. Lett.* **79**, 1249 (2001).
5. J. Ruan, P.M. Fauchet, L. Dal Negro, M. Cazzanelli and L. Pavesi, *Appl. Phys. Lett.* **83**, 5479 (2003).
6. M. Cazzanelli, D. Navarro-Urrios, F. Riboli, N. Daldosso, L. Pavesi, J. Heitmann, L.X. Yi, R. Scholz, M. Zacharias and U. Gösele, *J. Appl. Phys.* **96**, 3164 (2004).

7. L. Khriachtchev, M. Räsänen and S. Novikov, *Appl. Phys. Lett.* **83**, 3018 (2003).
8. J. Valenta, T. Ostatnický, I. Pelant, R.G. Elliman, J. Linnros and B. Hönerlage, *J. Appl. Phys.* **96**, 5222 (2004).
9. L. Khriachtchev, M. Räsänen, S. Novikov and J. Lahtinen, *J. Appl. Phys.* **95**, 7592 (2004).
10. L. Khriachtchev, S. Novikov, J. Lahtinen and M. Räsänen, *J. Phys.: Condens. Matter* **16**, 3219 (2004).
11. D. Navarro-Urrios, F. Riboli, Massimo Cazzanelli, A. Chiasera, N. Daldosso, L. Pavesi, C.J. Oton, J. Heitmann, L.X. Yi, R. Scholz and M. Zacharias, *Opt. Mater.* **27**, 763 (2005).
12. R. Ferre, B. Garrido, P. Pellegrino, M. Perálvarez, C. García, J. A. Moreno, J. Carreras and J. R. Morante, *J. Appl. Phys.* **98**, 084319 (2005).
13. J. Valenta, I. Pelant, K. Luterová, R. Tomasiunas, S. Cheylan, R.G. Elliman, J. Linnros and B. Hönerlage, *Appl. Phys. Lett.* **82**, 955 (2003).
14. P. Janda, J. Valenta, T. Ostatnický, E. Skopalová, I. Pelant, R.G. Elliman and R. Tomasiunas, *J. Lumin.* **121**, 267 (2006).
15. K. L. Shaklee, R. F. Leheny and R. E. Nahory, *Phys. Rev. Lett.* **26**, 888 (1971).
16. T. Ostatnický, J. Valenta, I. Pelant, K. Luterová, R.G. Elliman, S. Cheylan and B. Hönerlage, *Opt. Mater.* **27**, 782 (2005).
17. I. Pelant, T. Ostatnický, J. Valenta, K. Luterová, E. Skopalová, T. Mates and R.G. Elliman, *Appl. Phys. B* **83**, 87 (2006).
18. D. Marcuse, *Theory of Dielectric Optical Waveguides* (Academic Press, Boston, 1991).
19. A.W. Snyder and J.D. Love, *Optical Waveguide Theory* (Chapman&Hall, London, 1991).
20. R. E. Smith and S. N. Houde-Walter, *J. Opt. Soc. A* **12**, 715 (1995).
21. H. Kogelnik and V. Ramaswamy, *Appl. Opt.* **13**, 1867 (1974).
22. M. Born and E. Wolf, *Principles of Optics: Electromagnetic Theory of Propagation, Interference and Diffraction of Light* (Pergamon Press, Oxford, 1993).
23. The software package SRIM developed by J.F. Ziegler *et al*., http://www.srim.org.
24. K. Luterová, E. Skopalová, I. Pelant, M. Rejman, T. Ostatnický and J. Valenta, *J. Appl. Phys.* **100**, 074307 (2006).
25. T. Ostatnický, P. Janda, J. Valenta and I. Pelant, *Proc. SPIE* **6609**, 66090F (2007).
26. L. Dal-Negro, P. Bettotti, M. Cazzanelli, D. Pacifici and L. Pavesi, *Opt. Commun.* **229**, 337 (2004).
27. K. Luterová, D. Navarro, M. Cazzanelli, T. Ostatnický, J. Valenta, S. Cheylan, I. Pelant and L. Pavesi, *phys. stat. sol. (c)* **9**, 3429 (2005).
28. K. Luterová, M. Cazzanelli, J.-P. Likforman, D. Navarro, J. Valenta, T. Ostatnický, K. Dohnalová, S. Cheylan, P. Gilliot, B. Hönerlage, L. Pavesi and I. Pelant, *Opt. Mater.* **27**, 750 (2005).